



31 **Abstract**

32 The increasing availability of high-quality remote sensing data and advanced technologies have
33 spurred land cover mapping to characterize land change from local to global scales. However,
34 most land change datasets either span multiple decades at a local scale or cover limited time over
35 a larger geographic extent. Here, we present a new land cover and land surface change dataset
36 created by the Land Change Monitoring, Assessment, and Projection (LCMAP) program over
37 the conterminous United States (CONUS). The LCMAP land cover change dataset consists of
38 annual land cover and land cover change products over the period 1985-2017 at 30m resolution
39 using Landsat and other ancillary data via the Continuous Change Detection and Classification
40 (CCDC) algorithm. In this paper, we describe our novel approach to implement the CCDC
41 algorithm to produce the LCMAP product suite composed of five land cover and five land
42 surface change related products. The LCMAP land cover products were validated using a
43 collection of ~ 25,000 reference samples collected independently across CONUS. The overall
44 agreement for all years of the LCMAP primary land cover product reached 82.5%. The LCMAP
45 products are produced through the LCMAP Information Warehouse and Data Store (IW+DS)
46 and Shared Mesos Cluster systems that can process, store, and deliver all datasets for public
47 access. To our knowledge, this is the first set of published 30 m annual land cover and land cover
48 change datasets that span from the 1980s to the present for the United States. The LCMAP
49 product suite provides useful information for land resource management and facilitates studies to
50 improve the understanding of terrestrial ecosystems and the complex dynamics of the Earth
51 system. The LCMAP system could be implemented to produce global land change products in
52 the future.

53
54
55
56
57
58
59
60



61 **1 Introduction**

62

63 The characteristics of land surface fundamentally connect with the functioning of Earth's
64 terrestrial surface. Changes in land cover and land surface are one of the greatest and most
65 immediate influences on the Earth system and these changes will continue in association with a
66 surging human population and growing demand on land resources (Szantoi et al., 2020). Changes
67 in land cover and ecosystems and their implications for global environmental change and
68 sustainability are major research challenges for developing strategies to respond to ongoing
69 global change while meeting development goals (Turner II et al., 2007). Unknowns related to the
70 spatial extent and degrees of impacts of anthropogenic activities on natural systems and
71 strategies to respond to ongoing global change hinder efforts to overcome sustainability
72 challenges (Erb et al., 2017; Reid et al., 2010). An improved understanding of the complex and
73 dynamic interactions between the various Earth system components, including humans and their
74 activities, is critical for policymakers and scientists (Foley, 2005; Foley et al., 2011). To fully
75 understand these processes and monitor these changes, accurate and frequently updated land
76 cover information is essential for scientific research and to assist decision makers in responding
77 to the challenges associated with competing land demands and land surface change.

78 Satellite observations have been used to observe the Earth's surface and to characterize land
79 cover and change from local to global scales. Remote sensing data allows us to obtain
80 information over large areas in a practical and accurate manner. With advanced technologies and
81 accumulating satellite data, countries and regions have produced multi-spatial and multi-
82 temporal resolution land cover products (Chen et al., 2015; Gong et al., 2020; Hansen, 2013;
83 Homer et al., 2020; Li et al., 2020). A variety of land change mapping has been carried out to
84 produce land cover and change products in the United States. Among these efforts are the widely
85 known National Land Cover Database (NLCD) products. NLCD has provided comprehensive,
86 general-purpose land cover mapping products at 30-m resolution since 2001 in the United States,
87 and the products have been published and updated across more than a decade (Homer et al.,
88 2020). NLCD provides Anderson Level II land cover classification (Anderson, 1976) for the
89 conterminous United States (CONUS) at approximately 2–3-year intervals. Other national-scale
90 mapping projects focus on specific land cover themes. Among these are the Landscape Fire and
91 Resource Management Planning Tools (LANDFIRE) (Picotte et al., 2019), which maps



92 vegetation and fuels in support of wildfire management, and the Cropland Data Layer (Boryan et
93 al., 2011) generated by the National Agricultural Statistics Service (NASS) of the United States
94 Department of Agriculture (USDA). Due to the need to incorporate data from neighboring years,
95 as well as extensive post-processing, ancillary dataset dependencies, and analyst-supported
96 refinement, release dates for both LANDFIRE and NLCD products are typically several years
97 subsequent to the nominal map year. Other products including national urban extent change and
98 vegetation phenology data are available (Li et al., 2019; Li et al., 2020). These projects vary in
99 how land change information is incorporated or expressed across product releases. Continuous
100 data stacks allow for an increase in input features for land cover classification. Frequent data also
101 provides the opportunity for near-real time change monitoring with frequently updated image
102 acquisitions. The availability of land change information has led to approaches that attempt to
103 monitor surface properties continuously through time. Such approaches have several advantages
104 over traditional image processing techniques based on small numbers of images (Bullock et al.,
105 2020; Zhu and Woodcock, 2014b).

106 Leveraging the increasingly massive amount of openly available, analysis-ready data products
107 into the generation of operational land cover and land change information has been described as
108 the new paradigm for land cover science (Wulder et al., 2018). The approach, which intended to
109 use all available medium resolution remotely sensed data from the 1980s to the present, opened a
110 door for the scientific community to integrate time series information to improve change
111 detection and land cover characterization in a robust way. Furthermore, change events, when
112 combined with knowledge of ecology settings or anticipation of a given process post-change, can
113 accommodate consistent change observations and characterization of land cover. For example,
114 forest areas that are cleared by wildfire or harvest activities typically transfer to non-forest
115 herbaceous or shrub vegetation cover, followed by a succession of young tree stages, ultimately
116 returning to a forest class. Traditional change detection methods using limited observations may
117 not have identified these changes if data were collected with a starting date prior to the change
118 and an ending date that occurred after the transitional (non-tree) vegetation returned to tree
119 cover. Therefore, incorporating change information into the land cover characterization process
120 allows for insights regarding expected land cover class transitions related to successional
121 processes, and likewise provides a mechanism to identify illogical class transitions and cause or
122 agent of change (Kennedy et al., 2015; Wulder et al., 2018). The choice of a time series



123 approach also allows missing data and phenological variations to be handled robustly (Friedl et
124 al., 2010; Wulder et al., 2018).

125 The Continuous Change Detection (CCD) and Classification (CCDC) algorithm (Zhu and
126 Woodcock, 2014b; Zhu et al., 2015b) was developed to advance time series change detection by
127 using all available Landsat data. The CCD algorithm uses robust methodology to identify when
128 and how the land surface changes through time. The algorithm first estimates a time series model
129 based on clear observations and then detects outliers by comparing model estimates and Landsat
130 observations. The algorithm fits harmonic regression models through a Least Absolute Shrinkage
131 and Selection Operator (LASSO) (Tibshirani, 1996) approach to every pixel over time to
132 estimate the time series model defined by sine and cosine functions. New Landsat records are
133 compared to predicted results, and if the observed data deviate beyond a set threshold for all
134 records within a moving window period, then a model break is produced. The parameters used to
135 fit the model are used as inputs for the cover classifier for land cover characterization.

136 The original implementation of CCDC was written in the MATLAB programming language and
137 had been implemented for a regional land cover change assessment in the eastern CONUS (Zhu
138 and Woodcock, 2014b). The algorithm includes the automation of change detection/classification
139 and can monitor changes for different land cover types. The implementation of CCDC into a
140 large geographic extent still encounters several challenges: the availability of Landsat records
141 and training datasets, the effectiveness of choosing good quality Landsat records, and the
142 robustness to characterize land cover and change across various land cover types and conditions.
143 In this paper, we outlined major efforts and challenges in the implementation of CCDC for the
144 U.S. Geological Survey (USGS) Land Change Monitoring, Assessment, and Projection
145 (LCMAP) initiative (Brown et al., 2020). LCMAP focuses on using CCD/CCDC with time series
146 Landsat records and other ancillary information to produce annual land cover and change
147 products from 1985 to the present for the United States. We focused on how LCMAP employed
148 every observation in a time series of U.S. Landsat Analysis Ready Data (ARD) (Dwyer et al.,
149 2018) over a long period starting with the 1980s to determine whether change occurred at any
150 given point in the observation record. The algorithm was further used to classify the pixel to
151 indicate what land cover type(s) were observed before and after a detected change on the land
152 surface. The CCDC algorithm has since been translated into an open-source library as Python



153 code. The full implementation joined the CCD Python library with the classification
154 methodology in combination with data delivery/processing services made available through the
155 LCMAP Information Warehouse and Data Store (IW+DS).

156

157 **2 Data Sources**

158 The CCDC algorithm utilizes all available Landsat observations including surface reflectance,
159 brightness temperature, and associated quality data to characterize the spectral responses of
160 every pixel through harmonic regression model fits. The model fits are then used to categorize
161 each pixel time series into temporal segments of stable periods and to estimate the dates at which
162 the spectral time-series data diverge from past responses or patterns. The outcomes of model fits
163 and other input data are then used for classification. The algorithm requires several input datasets
164 to perform both change detection and classification.

165 **2.1 Landsat observations**

166 U.S. Landsat ARD have been processed to a minimum set of requirements and organized into a
167 form that can be more directly and easily used for monitoring and assessing landscape change
168 with minimal additional user effort. Landsat ARD Collection 1 provides consistent radiometric
169 and geometric Landsat products across Landsat 4-5 Thematic Mapper (TM), Landsat 7 Enhanced
170 Thematic Mapper Plus (ETM+), and Landsat 8 Operational Land Imager (OLI) / Thermal
171 Infrared Sensor (TIRS) instruments for use in time series analysis (Dwyer et al., 2018). Landsat
172 ARD is organized in tiles, which are units of uniform dimension bounded by static corner points
173 in a defined grid system (Fig. 1). An ARD tile is currently defined as 5,000 x 5,000 30-meter (m)
174 pixels or 150 x 150-kilometer (km). To implement CCDC algorithms to produce LCMAP
175 Collection 1.0 land change products in CONUS, all available Landsat ARD records of surface
176 reflectance and brightness temperature from the 1980s to 2017 were required.

177 **2.2 Land cover and ancillary datasets**

178 The CCDC algorithm employs every observation in a time series of Landsat data to determine
179 whether change has occurred at any given time. The algorithm further classifies the time series to
180 indicate what land cover types were observed before and after a detected change and further to
181 generate LCMAP annual land cover products (Table 1). The land cover products are produced by



182 using training data from NLCD in 2001. NLCD provides Anderson Level II (Anderson, 1976)
183 land cover classification for CONUS and outlying areas (Homer et al., 2020). Spectral index and
184 change metrics between cloud-corrected Landsat mosaics are used, among other information, to
185 identify change pixels (Jin et al., 2013). These metrics allow NLCD to incorporate temporal and
186 spectral trajectory information into both training data selection and final land cover
187 classification. The NLCD land cover data is used in LCMAP as land cover training data.

188

189 Ancillary data comprises two main source datasets: the USGS National Elevation Dataset (NED)
190 (Gesch et al., 2002) 1 arc-second Digital Elevation Models (DEM), and a wetland potential index
191 (WPI) layer created for NLCD 2011 land cover production (Zhu et al., 2016). The WPI layer is a
192 ranking (0–8) of wetland likelihood from a comparison of the National Wetland Inventory
193 (NWI), the U.S. Department of Agriculture Soil Survey Geographic Database (SSURGO) for
194 hydric soils, and the NLCD 2006 wetlands land cover classes.

195

196 **3 Methodology**

197 As part of the operational LCMAP system, the original MATLAB version of the CCDC
198 algorithm is converted to a format that meets the needs of large-scale land change detection and
199 change characterization on an annual basis. Python is selected to replace MATLAB to implement
200 the CCDC algorithm for LCMAP. The CCD component of the CCDC algorithm is converted to
201 create the Python-based CCD (PyCCD) library. The PyCCD library is a per-pixel algorithm, and
202 the fundamental outputs are the spectral characterizations (segments) of the input data. There are
203 several key components in PyCCD. The overall CCD procedures are summarized in Fig. 2.

204 **3.1 Data filtering and Harmonic modeling**

205 The removal of invalid and cloud-contaminated data points is important for deriving model
206 coefficients that accurately represent the phenology of the surface, and for the correct
207 identification of model break points. The CCD algorithm uses Landsat ARD PIXELQA values to
208 mask observations identified as cloud, cloud shadow, fill, or (in some cases) snow derived based
209 on the Fmask 3.3 algorithm (Zhu et al., 2015a; Zhu and Woodcock, 2012). Additional cirrus and
210 terrain occlusion bits are provided for Landsat 8 OLI-TIRS ARD that are not available in the



211 Landsat 4–7 TM/ETM+ quality assessment band. To maintain consistency across the historical
212 archive, the algorithm does not rely on these Landsat 8-only QA flags to filter out observations.

213 Landsat ARD containing invalid or physically unrealistic data values are removed. For the
214 surface reflectance bands, the valid data range is between 0 and 10000. Brightness temperature
215 values, which in the ARD are stored as $10 \times$ temperature (kelvin), are converted to $100 \times$ °C and
216 observations are filtered for values outside the range -9320 and 7070 (-93.2–70.7°C). This
217 procedure rescales the brightness temperature values into a roughly similar numerical range as
218 the surface reflectance bands. A multitemporal mask (Tmask) model (Zhu and Woodcock,
219 2014a) is implemented first to remove additional outliers by using the multitemporal observation
220 record to identify values that deviate from the overall phenology curve using a specific harmonic
221 model to perform an initial fit to the phenology. Additional details are provided in the
222 Supplementary materials S1.

223 The filtered Landsat ARD is further operated to generate the time series fit by harmonic models
224 whose sinusoidal components are frequency multiples of the base annual frequency. A constant
225 and linear term characterizes the surface reflectance or brightness temperature offset value and
226 overall slope, respectively. The full harmonic model is defined as follows:

$$227 \quad \hat{p}(i, t) = c_{0,i} + c_{1,i}t + \sum_{n=1}^3 (a_{n,i} \cos \omega nt + b_{n,i} \sin \omega nt) \quad (1)$$

228 where ω is the base annual frequency ($2\pi/T$), t is the ordinal of the date when January 1 of the
229 year zero has ordinal 1 (sometimes called Julian date), i is the i th Landsat band, $a_{n,i}$ and $b_{n,i}$ are
230 the estimated n th order harmonic coefficients for the i th Landsat band, $c_{0,i}$ and $c_{1,i}$ are the
231 estimated intercept and slope coefficients for the i th Landsat band, and $\hat{p}(i, t)$ is the predicted
232 value for the i th Landsat band at ordinal date t . Model initialization and certain special-case
233 regression fits such as at the beginning/end of the time series use the simple four-coefficient
234 model. Outside of these conditions, the selection of coefficient depends on the number of
235 observations used for the regression. For a full model (eight coefficients), there must be at least
236 24 observations covered by the regression. The fit parameters returned by PyCCD always
237 include eight coefficient values including an intercept, with unused coefficients reported as
238 zeroes.

239 **3.2 Regression models and change detection thresholds**



240 The best-fit coefficients for the time series model are calculated using a LASSO regression
241 model (Tibshirani, 1996). In contrast to Ordinary Least Squares (OLS) that was used in the
242 original CCDC development, LASSO penalizes the sum of the absolute values of coefficients, in
243 some cases forcing a subset of the coefficients to zero. Together with the explicit limits enforced
244 on the number of coefficients, this reduces instances of overfitting, including in cases when
245 observations are too sparse or unevenly distributed in time to constrain the model to real
246 phenological features. To detect change, the LASSO model checks CCD model breaks with
247 respect to its last determined best-fit harmonic model.

248 To correctly detect change, the algorithm distinguishes between a substantive deviation from
249 model prediction and deviations that result from variability inherent in the data (due to
250 incomplete atmospheric removal and/or other sources of natural variation) to detect change. The
251 algorithm calculates two parameters related to dispersion, or scatter, to estimate the variability of
252 data for each spectral band. The first one is a comparison root-mean-square-error (RMSE) that is
253 the RMSE of the 24 observations covered by the model which are closest in day of year to the
254 last observation in the “peek window,” or over all observations covered by the model if there are
255 fewer than 24. This value is recalculated at each step of the time series. The second parameter
256 (*var*) is used to measure the overall variability of the data values and is defined as the median of
257 the absolute value of the differences between each observation and the *i*th successive
258 observation, where *i* is the smallest value such that the majority of these observation pairs are
259 separated by greater than 30 days, if possible (otherwise, *i*=1). The *var* is computed once at the
260 beginning of the standard procedure, using all non-masked observations in the time series.

261 Observations not yet incorporated into the model are evaluated as a group of no fewer than the
262 *PEEK_SIZE* parameter value; this is the “peek window,” which “slides” along the time series
263 one observation at a time. Each iteration, a value is calculated for each individual observation
264 within the peek window, as follows:

$$mag_n = \sum_{i \in D} \left(\frac{resid_{n,i}}{\max(var_i, RMSE_i)} \right)^2 \quad (2)$$

265 where, $resid_{n,i}$ is the residual relative to the LASSO models for each band *i*, for each
266 observation *n* within the *PEEK_SIZE* window, var_i and $RMSE_i$ are the parameters of dispersion
267 as described above, for each band *i*. This summation is carried out for all bands *i* in the set of



268 *DETECTION_BANDS* (D). This produces a scalar magnitude, representing the deviation from
269 model prediction across these bands, for each observation. The detection of a model break
270 requires this value to be above the *CHANGE_THRESHOLD* value for all observations in the
271 window. This is separate from the value that is reported as a per-band magnitude when a change
272 is detected in the time series. Change detection sensitivity depends on the value of change
273 threshold. The *CHANGE_THRESHOLD* is determined in Eqs. S2 and S3 in the Supplementary.
274 If $mag_n < CHANGE_THRESHOLD$ for any n in the *Peek_Size* window, then add the most
275 recent observation to the segment by shifting the *Peek_Size* window one observation forward in
276 the time series. If $mag_n > CHANGE_THRESHOLD$ for all n in the *Peek_Size* window, this is
277 considered a spectral break.

278 **3.3 Permanent snow and insufficient clear observation procedures**

279 The permanent snow procedure indicates that too few clear (less than 25% of total observations)
280 or water observations, which are identified from the QA band, exist to robustly detect change,
281 and a large fraction of observations are snow. The algorithm will return at most one segment that
282 fits through the entire time series and provide the filtered observations number at least twelve.
283 The model will, under the default settings, fit only four coefficients (i.e., characterizing the
284 reflectance and brightness temperature bands using only a simple harmonic with no higher
285 frequency terms). Unlike other procedures, snow pixels are not filtered out and are fit as part of
286 the annual pattern. This avoids overfitting the model to a seasonally sparse observation record.
287 Similarly, for the insufficient clear observations determined by the QA band, the model will
288 perform a LASSO regression fit for the entire time series using four coefficients. The model
289 coefficients and RMSE from this regression are recorded. Additional parameters including the
290 start, end, and observation count are also saved. Further, the change Boolean value is set to 0,
291 and the break day is recorded as the last observation date. The magnitude of change as zero for
292 each band is also saved.

293 **3.4 Land cover classification**

294 The CCDC algorithm characterizes the land cover component of a pixel at any point using the
295 LCMAP time series model approach from the Landsat 4–8 records. The classification of CCDC
296 is accomplished for every pixel based on data from the time series models (e.g., model



297 coefficients). Land cover classifications are generated on an annual basis, using July 1st as a
298 representative date. A list of land cover classes and descriptions is provided in Table 1.

299 **3.4.1 Classification algorithm**

300 We chose eXtreme Gradient Boosting (XGBoost) (Chen and Guestrin, 2016) as the classification
301 method. XGBoost is a scalable implementation of gradient tree boosting, which is a supervised
302 learning method that can be used to develop a classification model when provided with an
303 appropriate training dataset. Generally, for a given dataset, a tree ensemble model uses additive
304 functions, which correspond to independent tree structures, to predict the land cover. The
305 predictions from all trees are also normalized to the final class probabilities using the softmax
306 function. The algorithm can handle sparse data and theoretically justify weighted quantile sketch
307 for approximate learning. The resultant trained model can be applied to a larger dataset to
308 generate predictions and probability scores which are the basis for LCMAP primary and
309 secondary land cover types. The primary and secondary land cover confidence values are
310 calculated from these scores.

311 **3.4.2 Training dataset**

312 The training data used in XGBoost for the LCMAP Collection 1.0 land cover products is from
313 the USGS NLCD 2001 land cover product (Homer et al., 2020). To meet the LCMAP land cover
314 legend, the NLCD data is first cross-walked to LCMAP classes, as shown in Fig.3 and Table 2.
315 The extent of each land cover in the cross-walked NLCD layer is eroded by one pixel. This step
316 aims to reduce potential noise in the classifier by removing pixels that may be heavily mixed
317 with different cover types, or whose land cover label may be less reliable. It also removes the
318 narrow linear low-intensity developed pixels corresponding to road networks, which were found
319 to have registration issues with Landsat ARD in some areas.

320

321 **3.4.3 Ancillary data**

322 Ancillary data used in the classification contains two main datasets: the DEM and the WPI layer.
323 Three DEM derivative datasets are implemented as geographic references for land cover
324 classification as ancillary data including topographic slope, aspect, and position index. The WPI



325 is highly related to wetland distribution and has a potential to improve wetland classification in
326 LCMAP.

327 **3.4.4 Classification procedures**

328 For each pixel, CCD segment data for the segment that includes the July 1st, 2001 date is used
329 with training data to create classification models (Zhou et al., 2020; Zhu et al., 2016). The CCD
330 model data used with training data include the model coefficients (except the intercepts)
331 generated from surface reflectance and brightness temperature bands, the model RMSE value for
332 each band, and an average intercept value that is calculated from average annual reflectance
333 values for each band for the July 1, 2001 year. The model training procedure is conducted at the
334 tile level, using random samples drawn from the targeted tile as well as the eight surrounding
335 tiles to avoid not having enough training samples of rare land cover types in the targeted tile.
336 Cross-walked and eroded NLCD data are used for classification labels, while the CCD model
337 outputs and ancillary data are provided as independent variables. Based on training data testing
338 using different sample sizes, a target sample size of 20 million pixels from the extent of 3x3
339 ARD tiles is chosen, requiring approximately proportional representation of classes with the
340 added constraint that no class be represented by fewer than 600,000 or more than 8 million
341 samples. If there are fewer than 600,000 samples available for a class, then all of the available
342 samples are used without any oversampling. The XGBoost hyperparameters are selected as:
343 maximum tree depth 8; fast histogram optimized approximate greedy algorithm for tree method;
344 multiclass logloss for evaluation metric; and maximum number of rounds 500.

345 After the classification models in a given tile are trained, predictions are generated for each July
346 1st date that has an associated CCD segment (Fig. 4). The prediction information is supplied to
347 the production step for the creation of land cover. The process is repeated for each tile for the
348 entire CONUS ARD extent.

349 **3.5 Validation data**

350 The LCMAP land cover product is validated using an independent reference dataset. The
351 reference data, which consists of 24,971 30 m x 30 m pixels selected via a simple random
352 sampling method over CONUS, is collected from these sample plots between 1985 and 2017.
353 The TimeSync tool is used to efficiently display Landsat data for interpretation and to record



354 these interpretations into a database (Cohen et al., 2010; Pengra et al., 2020a). TimeSync displays
355 the input Landsat images in two basic ways: by annual time-series images and by pixel values
356 plotted through time. For the image display, single 255 x 255-pixel subsets of Landsat images in
357 the growing season are displayed in sequence from 1984 to 2018. Trained interpreters have
358 access to all available images in each year to collect attributes in three basic categories: 1) land
359 use, 2) land cover, and 3) change processes. Additional attribute details for the change processes,
360 such as clear-cut and thinning associated with harvest events, are also collected. The interpreters
361 manually label these attributes using Landsat 5, 7, and 8 imagery, high-resolution aerial
362 photography, and other ancillary datasets (Cohen et al., 2010; Pengra et al., 2020a). Interpreters
363 also use ancillary data to support interpretation of Landsat and high-resolution imagery, although
364 Landsat data takes the highest weight of evidence. Recording the full set of attributes in land use,
365 land cover, and land change categories provides sufficient information to meet the needs of
366 LCMAP as well as other potential users. Quality assurance and quality control (QA/QC)
367 processes are also implemented to ensure the quality and consistency of the reference data
368 among interpreters and over the time span of data collection (Pengra et al., 2020a). The collected
369 samples are then cross-walked to the appropriate LCMAP land cover class, providing a single
370 land cover reference label for each year of the time series for each sample pixel.

371 The validation analysis protocols focus on estimating the confusion matrix and overall, user's,
372 and producer's accuracy by comparing the reference data and product data labels. Overall
373 accuracy and producer's accuracy as well as standard errors are produced using post stratified
374 estimators (Card, 1982; Stehman, 2013). For accuracy estimates that are produced by combining
375 multiple years of data, the sampling design is treated as a one-stage cluster sample where each
376 pixel represents a cluster and each year of observation is the secondary sampling unit using
377 cluster sampling standard error formulas (Pengra et al., 2020). The validation is only performed
378 for primary land cover and change products, not for other LCMAP science products
379 (Supplementary Section 4).

380 **3.6 Information warehouse and data store**

381 The LCMAP adopts an information warehouse and data store (IW+DS) system that can expand
382 storage solutions along with data access and discovery services running on the EROS Shared
383 Mesos Cluster. The system provides different storage solutions to allow for flexibility in



384 choosing what best fits a dataset's characteristics and currently comprises Apache Cassandra
385 (<https://cassandra.apache.org/>) and Ceph (<https://ceph.io/>) object storage. The services provide
386 data ingest, retrieval, discovery, metadata, processing, and other functionalities. LCMAP
387 maintains a copy of Landsat Collection 1 ARD and other similarly tiled ancillary datasets that
388 are spatially subset within the IW+DS to allow efficient retrieval and to enable large-scale
389 CCDC processing and other algorithmic work. The ingest process is designed to avoid bringing
390 in ARD tile observations that are already present within the IW+DS, to keep the input consistent
391 with any prior usage while allowing CCDC to bring in new observations as they are available.
392 Algorithmic results, products, and other intermediate data are kept on the Ceph object store
393 arranged using a prefix structure to label the identity of the data, with the actual object names
394 incorporating spatial concepts such as tile and chip that is a small subset of a tile and contains
395 100 by 100 30m pixels.

396

397 **4 Results and Discussion**

398

399 The LCMAP primary land cover and change products were evaluated to outline annual land
400 cover change from 1985 to 2017 in the conterminous Unites States.

401 **4.1 Collection 1.0 primary land cover distribution and change**

402 The CONUS primary land cover mapping result and the primary confidence in 2010 are shown
403 in Fig. 5a and b, respectively. The land cover map illustrates distributions of different land cover
404 types across CONUS. The primary confidence is above 90% for most land cover classes,
405 suggesting that the classification models were created with high confidence for land cover
406 mapping for most classes in most regions. Some vegetation transition (dark green in Fig. 5b)
407 occurs mainly in the southeast region suggesting gradual tree recovery from disturbances
408 associated with tree harvesting. Fig. 5c and d display numbers of land cover changes and spectral
409 changes detected by the CCDC model between 1985 and 2017. The number of land cover
410 changes represents how many times land cover has changed from one type to another for a
411 specific pixel. However, the number of spectral changes denotes how many times the model has
412 detected spectral changes in a CCD time series model where spectral observations have diverged
413 from the model predictions. These changes could relate to a change in thematic land cover or



414 might represent more subtle conditional surface changes. The southeast region shows more
415 frequent land cover changes in the 33 years (Fig. 5c). The western part of CONUS, however,
416 contains more spectral changes than in the east. The different spatial patterns in the total number
417 of land cover changes (Fig. 5c) and detected spectral changes (Fig. 5d) suggest that not all
418 changes lead to land cover change (e.g., drought and precipitation-related changes in vegetation
419 or grassland fire). The large numbers of spectral change were mainly detected in the southern
420 grassland area.

421 Fig. 6 shows the temporal changes of areas for eight land cover classes from 1985 to 2017.
422 Among all classes, grass/shrub, tree cover, and cropland were dominant land cover types,
423 followed by wetland, water, developed, barren, and snow/ice. The land cover and change
424 datasets show that developed land has a consistent increasing trend with an 8.4% increase while
425 barren increased 9.1% between 1985 and 2017. Overall, the developed and barren areas
426 increased 2.58×10^4 km² and 8.56×10^3 km², respectively. Other land cover categories do not have
427 such increasing patterns. As for water, although fluctuating, it had a generally increasing trend.
428 The area of wetland had a rapid decrease before 2000, following a relatively steady though
429 fluctuating trend. Net wetland extent declined about 0.4% from 1985 to 2017. The grass/shrub
430 and tree cover classes both experienced consistent increasing trends before 2008 and 1995 with
431 areas reaching about 2.85×10^6 km² for grass/shrub and 2.14×10^6 km² for tree in these two years
432 These two land covers gradually decreased since then. Tree cover declines after 1996, showing a
433 decreasing rate of 2.8% between 1985 and 2017. The cropland decreased from 1985 to 2008 and
434 quickly increased after that. By 2017, the area of cropland reached a similar level of cropland
435 area in 1988. Furthermore, most land cover changes are located in the southeast region where
436 many pixels change more than one time. The changes detected by the CCD model suggest that
437 landscape in the Midwest and west are more dynamic than in the east. Many areas experience
438 multiple disturbances although most of these changes do not result in land cover transition.

439 The south ARD tile outlined in Fig. 5(a) covers the northern Dallas region, and the spatial
440 patterns of land cover and change are shown in more detail in Fig. 7. The land cover distributions
441 in the region show that urban land expands considerably from 1985 (Fig. 7a), to 1990 (Fig. 7b),
442 and to 2016 (Fig. 7c). The land conversion was primarily from cropland and grass/shrub to
443 developed land. Lake Ray Roberts was created in the late 1980s and captured in the land cover



444 map (Fig. 7b&c). The lake and urban conversion are also visible in the change count from 1985
445 to 2016 (Fig. 7g), which mainly show as blue, suggesting a one-time conversion. On the other
446 hand, there is almost no change in the urban center (Fig. 7g). Fig. 7 (d-f) shows high
447 classification confidence at the urban center, water, grass/shrub, and tree cover areas, whereas
448 cropland has relatively low confidence, indicating frequent management activities over croplands
449 in the regions. The total pixels of different change numbers suggest that one to two change times
450 are dominant, although some pixels change more than three times (Fig. 7h). The land cover
451 distributions in 1985, 1990, and 2017 show an increase in developed land and decreases in
452 cropland and grass/shrub (Fig. 7i).

453 The spatial patterns of land cover and change in the north ARD tile displayed in Fig. 5(a) in
454 northern Wyoming are shown in Fig. 8. The tile covers most of Yellowstone National Park, in
455 which tree, grass/shrub, and water are three dominant land cover types. Land cover in 1985,
456 1990, and 2016 (Fig. 8a-c) changed from tree to grass/shrub and back to tree cover. The primary
457 land cover confidence layers exhibit changes as decreasing vegetation from tree to grass/shrub
458 and increasing vegetation from grass/shrub to tree (Fig. 8d-f). For those trees and water bodies
459 that did not experience any disturbances, their magnitudes of confidence are relatively large. The
460 change map suggests that most forest lands experienced at least one change and some areas
461 changed multiple times (Fig. 8g). Most changes in forest lands were related to wildland fires that
462 occurred in the region. In 1988, 50 fires burned a mosaic covering nearly 3213 km² in
463 Yellowstone as a result of extremely warm, dry, and windy weather (NPS, 2021). Trees regrew
464 in some of the burn areas and these changes could occur more than once as shown in the change
465 map that indicates at least two changes in these areas. The total pixels of different change
466 frequencies suggest that one to two changes were dominant and very few pixels changed more
467 than three times (Fig. 8h). The land cover distributions in 1985, 1990, and 2017 had increases in
468 grass/shrub after 1985 and reductions in tree cover after that (Fig. 8i).

469 **4.2 Validation of land cover product**

470 The overall accuracy between the annual reference land cover label and the LCMAP annual land
471 cover products was calculated as 82.5% ($\pm 0.22\%$, standard error) when summarized for all years.
472 Overall accuracy across the time series (1985-2017) varied within about 1.5% annually, ranging
473 from a high of 83% in the late 1990s to about 82% in the late 2010s (Fig. 9). Per class accuracies



474 across CONUS ranged between 43% and 96% for user's accuracy (Table 3), with water showing
475 the highest accuracy ($96\% \pm 0.5\%$ user's accuracy and $93\% \pm 0.7\%$ producer's accuracy).
476 Cropland has about 93% ($\pm 0.3\%$) producer's accuracy and 70% ($\pm 0.6\%$) user's accuracy. The
477 lowest accuracies are observed for barren and wetland. The per class per year agreements show
478 the accuracies vary slightly for each class in each year (Table 4).

479 **4.3 Significance of the product**

480 One of the biggest advances of LCMAP relative to conventional methods available to date is its
481 approach of generating annual land change products by using the entire Landsat archive at a
482 large geographic scale. Landsat ARD, which is the foundation for LCMAP, is effective and
483 straightforward for tracking and characterizing the historical land changes at a pixel level over
484 decades. Compared to conventional methods, detecting changes using all available observations
485 enables us to date these changes as they occur. After change is detected, temporally consistent
486 land cover products rather than stochastic changes in labels can be produced at annual intervals
487 by conducting classification from CCD model segmented contributions

488 The LCMAP product suite includes five land cover change and five land surface change science
489 products. It represents a new paradigm that consistently and continuously provides a large
490 volume of land change information for land change monitoring, land resource management, and
491 scientific research. In addition to primary and secondary land cover before and after changes,
492 change segments containing spectral change time and magnitude are provided to explore the
493 changes in land condition and could meet various user communities' needs. The LCMAP
494 products can improve our understanding of causes, rates, and consequences of the land surface
495 changes (Rover et al. 2020) such as forest changes caused by wildfire and insect outbreaks.

496 By implementing the CCDC algorithm through a system engineering approach, LCMAP
497 provides a fully automated framework for land change monitoring. The framework can also be
498 updated to include the latest Landsat records so that it can be used for operational continuous
499 monitoring in a large geographic extent (Brown et al. 2020). Therefore, when new observations
500 become available, the framework can provide timely and consistent land cover characteristics to
501 the public.

502 **4.4 Limitations and challenges**



503 Although LCMAP Collection 1.0 products have been proven to be successful in detecting
504 various land surface changes to support research applications related to environment and ecology
505 conditions, limitations and challenges exist. Utilizing Landsat ARD data as input provided
506 consistent time series Landsat imagery with high level geometric and radiometric quality for
507 implementing the CCDC method. Nevertheless, the densities of Landsat observation records
508 varied greatly across space and time due to spatial differences in Landsat scene overlap and
509 temporal coverage, as well as regional differences in contamination by clouds, cloud shadows,
510 and snow. The change detection accuracies of CCD models were highly influenced by the
511 temporal frequency of available observations. Zhou et al. (2019) found that using harmonized
512 Landsat-8 and Sentinel-2 (HLS) data increased the temporal frequency of the data and thus
513 enhanced the ability to model seasonal variation and derived better change detection results than
514 using Landsat data alone. Integrating multi-mission data could provide the opportunity to
515 enhance change detection, especially for the land cover types that are highly dynamic or in
516 frequently cloudy/snowy areas.

517 Providing only eight general land cover classes and their changes in LCMAP Collection 1.0
518 products limits the usage of the product in some applications that need a higher level of thematic
519 land cover detail. For example, shrub and grass are two major vegetation types and have
520 different ecological functions but they are not delineated separately in LCMAP Collection 1.0
521 products. Lack of measurement of grassland-shrub transition constrains the study of shrub
522 encroachment, which is a symptom of land degradation.

523 Adopting NLCD 2001 as the training data source efficiently provided abundant training samples
524 to deliver land cover product with high classification accuracy. However, these training data
525 were randomly selected from the NLCD land cover product, suggesting errors could potentially
526 be carried over to the training samples due to potential errors in the training source. Besides
527 uncertainties in training data, some obvious challenges such as class definitional differences
528 between pasture/hay and grassland between NLCD and LCMAP could potentially be carried
529 over to the LCMAP land cover product. Implementing training data by reducing uncertainties
530 and potential errors in a more consistent and accurate way is critical to strengthen land cover
531 classification and to improve the scientific quality of LCMAP products in the future.



532 There are apparent shifts in some land cover types, especially in snow/ice and barren (Fig.6), and
533 a decline in overall agreement (Fig.9) in 2017, the last year of the Collection 1.0 product. The
534 last year's product usually is provisional because limited Landsat observations are available at
535 the end of a time series. The CCDC requires at least 24 clear observations to create full models
536 for change detection and classification. Without sufficient clear observations, the algorithm
537 could not produce model break accurately. Therefore, in the last year of a time series, the rule-
538 based assignment is implemented to label land cover for these pixels that do not have enough
539 observations to build a time series model. Both primary and secondary land cover classes are
540 assigned from the last identified primary and secondary classes.

541

542 **5 Data Availability**

543 The LCMAP products generated in this paper are available at <https://earthexplorer.usgs.gov/>
544 (LCMAP, 2021). All LCMAP land change products are mosaiced for the conterminous United
545 States in the GeoTIFF format. Find exact data as described here at
546 <https://doi.org/10.5066/P9W1TO6E>. The reference dataset used for the product validation is also
547 available at <https://www.sciencebase.gov/catalog/item/5e57e965e4b01d50924a93f6>
548 or <https://doi.org/10.5066/P98EC5XR> (Pengra et al., 2020b).

549

550 **6 Conclusions**

551 The continuous Landsat observations spanning from the 1980s to the present, new generations of
552 change detection and classification models, and systems capable of processing large volume data
553 are offering unprecedented opportunities to characterize land cover and detect land surface
554 change consistently and accurately. Additionally, the collection of reference data used to validate
555 land cover products provides validation result for each land cover category annually. To capture
556 the variability of landscape condition and its responses to different disturbances, land cover and
557 land surface change datasets need to be produced over a large geographic scale. The LCMAP has
558 produced a suite of land change product in 30 m resolution including the reference dataset in the
559 United States. In that context, LCMAP was developed to generate an essential dataset to meet
560 broad scientific research and resource management needs. Using the CCDC algorithm and



561 Landsat ARD to determine whether change has occurred at any given point in the observation
562 record, LCMAP produced annual land cover and change datasets for the conterminous United
563 States in a robust manner. These new datasets and the novel production systems will allow for
564 new generation of research and applications in connecting time series remote sensing
565 observations with land surface change at a much finer scale than previously possible.

566

567 **Supplement.** The supplement related to this article is attached.

568

569 **Author contributions.**

570 KS conducted PyCCD programming for CCD/CCDC models. ZZ developed the original
571 MATLAB version of CCD/CCDC programs. JH participated in reference data collection. DW
572 and QZ assisted in data integration tasks. GX analysed the data and wrote the manuscript with
573 contributions from all co-authors.

574

575 **Completing interests.** The authors declare that they have no conflict of interest.

576

577 **Acknowledgements.**

578 Any use of trade, firm, or product names is for descriptive purposes only and does not imply
579 endorsement by the U.S. Government. Qiang Zhou and Congcong Li's work were performed
580 under Work performed under USGS contract 140G0119C0001.

581

582

583



References

- Anderson, J. R., Hardy, E.E., Roach, J.T., and Witmer, R.E.: A land use and land cover classification system for use with remote sensor data, Geological Survey Professional Paper, 964, 1-28, 1976.
- Boryan, C., Yang, Z., Mueller, R., and & Craig, M.: Monitoring US agriculture: the US department of agriculture, national agricultural statistics service, cropland data layer program, Geocarto International, 26, 341-358, 2011.
- Brown, J. F., Tollerud, H. J., Barber, C. P., Zhou, Q., Dwyer, J. L., Vogelmann, J. E., Loveland, T. R., Woodcock, C. E., Stehman, S. V., Zhu, Z., Pengra, B. W., Smith, K., Horton, J. A., Xian, G., Auch, R. F., Sohl, T. L., Saylor, K. L., Gallant, A. L., Zelenak, D., Reker, R. R., and Rover, J.: Lessons learned implementing an operational continuous United States national land change monitoring capability: The Land Change Monitoring, Assessment, and Projection (LCMAP) approach, Remote Sensing of Environment, 238, 111356, 2020.
- Bullock, E. L., Woodcock, C. E., and Holden, C. E.: Improved change monitoring using an ensemble of time series algorithms, Remote Sensing of Environment, 238, 2020.
- Chen, J., Liao, A., Cao, X., Chen, L., Chen, Z., He, C., Han, G., Peng, S., Lu, M., and Zhang, W.: Global land cover mapping at 30 m resolution: A POK-based operational approach, ISPRS journal of photogrammetry and remote sensing : official publication of the International Society for Photogrammetry and Remote Sensing, 103, 7-27, 2015.
- Chen, T. and Guestrin, C.: XGBoost, Proceedings of the 22nd ACM SIGKDD International Conference on Knowledge Discovery and Data Mining, 785-794, 2016.
- Cohen, W. B., Yang, Z., and & Kennedy, R.: Detecting trends in forest disturbance and recovery using yearly Landsat time series: 2. TimeSync — Tools for calibration and validation, Remote Sensing of Environment, 114, 2911-2924, 2010.
- Dwyer, J. L., Roy, D. P., Sauer, B., Jenkerson, C. B., Zhang, H. K., and Lymburner, L.: Analysis Ready Data: Enabling Analysis of the Landsat Archive, Remote Sensing, 10, 1363, 2018.
- Erb, K. H., Luysaert, S., Meyfroidt, P., Pongratz, J., Don, A., Kloster, S., Kuemmerle, T., Fetzel, T., Fuchs, R., Herold, M., Haberl, H., Jones, C. D., Marin-Spiotta, E., McCallum, I., Robertson, E., Seufert, V., Fritz, S., Valade, A., Wiltshire, A., and Dolman, A. J.: Land management: data availability and process understanding for global change studies, Glob Chang Biol, 23, 512-533, 2017.
- Foley, J. A., DeFries, R., Asner, G.P., Barford, C., Bonan, G., Carpenter, S.R., Chapin, F.S., Coe, M.T., Daily, G.C., Gibbs, H.K., Helkowski, J.H., Holloway, T., Howard, E.A., Kucharik, C.J., Monfreda, C., Patz, J.A., Colin Prentice, I., Ramankutty, N., Synder, P.K.: Global consequences of land use, Science, 309, 570-574, 2005.
- Foley, J. A., Ramankutty, N., Brauman, K. A., Cassidy, E. S., Gerber, J. S., Johnston, M., Mueller, N. D., O'Connell, C., Ray, D. K., West, P. C., Balzer, C., Bennett, E. M., Carpenter, S. R., Hill, J., Monfreda, C., Polasky, S., Rockstrom, J., Sheehan, J., Siebert, S., Tilman, D., and Zaks, D. P.: Solutions for a cultivated planet, Nature, 478, 337-342, 2011.
- Friedl, M. A., Sulla-Menashe, D., Tan, B., Schneider, A., Ramankutty, N., Sibley, A., and Huang, X.: MODIS Collection 5 Global Land Cover: Algorithm Refinements and Characterization of New Datasets, Remote Sensing of Environment, 114, 168-182, 2010.
- Gong, P., Li, X., Wang, J., Bai, Y., Chen, B., Hu, T., Liu, X., Xu, B., Yang, J., Zhang, W., and and Zhou, Y.: Annual maps of global artificial impervious areas (GAIA) between 1985 and 2018, Remote Sensing of Environment, 236, 111510, 2020.



- Hansen, M. C., Potapov, P.V., Moore, R., et al.: High-resolution global maps of 21st century forest cover change, *Science*, 342, 850-853, 2013.
- Homer, C., Dewitz, J., Jin, S., Xian, G., Costello, C., Danielson, P., Gass, L., Funk, M., Wickham, J., Stehman, S., Auch, R., and Riitters, K.: Conterminous United States land cover change patterns 2001–2016 from the 2016 National Land Cover Database, *ISPRS Journal of Photogrammetry and Remote Sensing*, 162, 184-199, 2020.
- Jin, S., Yang, L., Danielson, P., Homer, C., Fry, J., and Xian, G.: A comprehensive change detection method for updating the National Land Cover Database to circa 2011, *Remote Sensing of Environment*, 132, 159-175, 2013.
- Kennedy, R. E., Yang, Z., Braaten, J., Copass, C., Antonova, N., Jordan, C., and Nelson, P.: Attribution of disturbance change agent from Landsat time-series in support of habitat monitoring in the Puget Sound region, USA, *Remote Sensing of Environment*, 166, 271-285, 2015.
- LCMAP, LCMAP Collection 1 Science Products [data]. <https://doi.org/10.5066/P9W1TO6E>, 2021.
- Li, X., Zhou, Y., Meng, L., Asrar, G. R., Lu, C., and Wu, Q.: A dataset of 30 m annual vegetation phenology indicators (1985–2015) in urban areas of the conterminous United States, *Earth System Science Data*, 11, 881-894, 2019.
- Li, X., Zhou, Y., Zhu, Z., and Cao, W.: A national dataset of 30 m annual urban extent dynamics (1985–2015) in the conterminous United States, *Earth System Science Data*, 12, 357-371, 2020.
- NPS, 2021. Fire - Yellowstone National Park, <https://www.nps.gov/yell/learn/nature/fire.htm#:~:text=Number%20in%20Yellowstone,human%2Dcaused%20fires%20were%20suppressed.&text=The%20number%20of%20fires%20has,70%2C285%20acres%20in%20Yellowstone%20burned>. Accessed in April 27, 2021.
- Pengra, B. W., Stehman, S. V., Horton, J. A., Dockter, D. J., Schroeder, T. A., Yang, Z., and Loveland, T. R.: Quality control and assessment of interpreter consistency of annual land cover reference data in an operational national monitoring program, *Remote Sensing of Environment*, 238, 111261, 2020a.
- Pengra, B.W., Stehman, S.V., Horton, J.A., and Wellington, D.F., 2020, Land Change Monitoring, Assessment, and Projection (LCMAP) Version 1.0 Annual Land Cover and Land Cover Change Validation Tables: U.S. Geological Survey data release, [data], <https://doi.org/10.5066/P98EC5XR>, 2020b.
- Picotte, J. J., Dockter, D., Long, J., Tolk, B., Davidson, A., and Peterson, B.: LANDFIRE remap prototype mapping effort: Developing a new framework for mapping vegetation classification, change, and structure, *Fire*, 2, 35, 2019.
- Reid, W. V., Chen, D., Goldfarb, L., Hackmann, H., Lee, Y. T., Mokhele, K., Ostrom, E., Raivio, K., Rockstrom, J., Schellnhuber, H. J., and Whyte, A.: Earth System Science for Global Sustainability: Grand Challenges, *Science*, 330, 916-917, 2010.
- Szantoi, Z., Geller, G. N., Tsendbazar, N.-E., See, L., Griffiths, P., Fritz, S., Gong, P., Herold, M., Mora, B., and Obregón, A.: Addressing the need for improved land cover map products for policy support, *Environmental Science & Policy*, 112, 28-35, 2020.
- Tibshirani, R.: Regression shrinkage and selection via the lasso, *Journal of the Royal Statistical Society: Series B (Methodological)*, 58, 267-288, 1996.
- Turner II, B. L., Lambin, E. F., and and Reeberg, A.: The emergence of land change science for global environmental change and sustainability, *Proceedings of the National Academy of Sciences of the United States of America*, 104, 20666-20671, 2007.



- Wulder, M. A., Coops, N. C., Roy, D. P., White, J. C., and Hermosilla, T.: Land cover 2.0, *International Journal of Remote Sensing*, 39, 4254-4284, 2018.
- Zhou, Q., Tollerud, H. J., Barber, C. P., Smith, K., and Zelenak, D.: Training data selection for annual land cover classification for the land change monitoring, assessment, and projection (LCMAP) initiative, *Remote Sensing*, 12, 699, 2020.
- Zhu, Z., Gallant, A. L., Woodcock, C. E., Pengra, B., Olofsson, P., Loveland, T. R., Jin, S., Dahal, D., Yang, L., and R.F., a. A.: Optimizing selection of training and auxiliary data for operational land cover classification for the LCMAP initiative, *ISPRS Journal of Photogrammetry and Remote Sensing* 122, 206-221, 2016.
- Zhu, Z., Wang, S., and Woodcock, C. E.: Improvement and expansion of the Fmask algorithm: Cloud, cloud shadow, and snow detection for Landsats 4–7, 8, and Sentinel 2 images, *Remote Sensing of Environment*, 159, 269-277, 2015a.
- Zhu, Z. and Woodcock, C. E.: Automated cloud, cloud shadow, and snow detection in multitemporal Landsat data: An algorithm designed specifically for monitoring land cover change, *Remote Sensing of Environment*, 152, 217-234, 2014a.
- Zhu, Z. and Woodcock, C. E.: Continuous change detection and classification of land cover using all available Landsat data, *Remote Sensing of Environment*, 144, 152-171, 2014b.
- Zhu, Z. and Woodcock, C. E.: Object-based cloud and cloud shadow detection in Landsat imagery, *Remote Sensing of Environment*, 118, 83-94, 2012.
- Zhu, Z., Woodcock, C. E., Holden, C., and Yang, Z.: Generating synthetic Landsat images based on all available Landsat data: Predicting Landsat surface reflectance at any given time. , *Remote Sensing of Environment*, 162, 67-83, 2015b.



Caption of Table

Table 1 LCMAP land cover product specifications

Table 2 NLCD land cover cross-walked to LCMAP land cover

Table 3. Confusion matrix for CONUS (all years combined) where cell entries represent percent of CONUS area. Overall accuracy is 82.5% ($\pm 0.22\%$). Standard errors for user's and producer's accuracies are shown in parentheses and n is the number of sample pixels for each row and column.

Table 4 Overall per class agreement in percentage between 1985 and 2017

Caption of Figure

Figure 1 Landsat ARD tile grids for the conterminous U.S.

Figure 2 Overall procedures of the CCD algorithm.

Figure 3. Figure 3. NLCD 2001 land cover (a), cross-walked LCMAP land cover classes (b), LCMAP land cover eroded by one pixel (c), zoomed in cross-walked land cover from NLCD 2001 (d), and zoomed in LCMAP land cover classes eroded by one pixel (e). The color legends represent NLCD land cover class and LCMAP primary land cover (LCPRI).

Figure 4 CCD change detection and segmentation using Landsat blue, green, red, near-infrared, short-wave infrared (SWIR) 1, short-wave infrared (SWIR) 2, and thermal bands. Blue dots are all available clear Landsat records in each year. The horizontal lines in different colors represent land cover classes labeled by the algorithm. The vertical lines show model break dates. The back line is the model fits. The high-resolution images show landscape conditions in 2007 and 2013.

Figure 5 Illustration of the LCMAP product: (a) Primary land cover in 2010, (b) Primary land cover confidence in 2010, (c) total number of land cover changes from 1985 to 2017, and (d) total number of changes detected from 1985 to 2017.

Figure 6 Areal variations of eight primary land cover types from 1985 to 2017 in CONUS.

Figure 7 Primary land cover and confidences in 1985 (a) and (d), 1990 (b) and (e), 2016(c) and (f), change in 1985-2017 (g), total pixels of different change (h), and areas of different land cover in the three times for the ARD tile 16_14 (i).

Figure 8 Primary land cover and confidences in 1985 (a) and (d), 1990 (b) and (e), 2016 (c) and (f), and change in 1985-2017 (g), total pixels of different change (h), and areas of different land cover in the three times for the ARD tile 9_6 (i).

Figure 9 Overall agreement between LCMAP primary land cover and reference data across CONUS. The cross lines represent \pm one standard errors.



Table 1 LCMAP land cover product specifications

Code	Land Cover Class	Description
1	Developed	Areas of intensive use with much of the land covered with structures (e.g., high-density residential, commercial, industrial, mining, or transportation), or less intensive uses where the land cover matrix includes vegetation, bare ground, and structures (e.g., low-density residential, recreational facilities, cemeteries, transportation/utility corridors, etc.), including any land functionality related to the developed or built-up activity.
2	Cropland	Land in either a vegetated or unvegetated state used in production of food, fiber, and fuels. This includes cultivated and uncultivated croplands, hay lands, orchards, vineyards, and confined livestock operations. Forest plantations are considered as forests or woodlands (Tree Cover class) regardless of the use of the wood products.
3	Grass/Shrub	Land predominantly covered with shrubs and perennial or annual natural and domesticated grasses (e.g. pasture), forbs, or other forms of herbaceous vegetation. The grass and shrub cover must comprise at least 10% of the area and tree cover is less than 10% of the area.
4	Tree Cover	Tree-covered land where the tree cover density is greater than 10%. Cleared or harvested trees (i.e. clearcuts) will be mapped according to current cover (e.g. Barren, Grass/Shrub).
5	Water Bodies	Areas covered with water, such as streams, canals, lakes, reservoirs, bays, or oceans.
6	Wetland	Lands where water saturation is the determining factor in soil characteristics, vegetation types, and animal communities. Wetlands are composed of mosaics of water, bare soil, and herbaceous or wooded vegetated cover.
7	Ice and Snow	Land where accumulated snow and ice does not completely melt during the summer period (i.e. perennial ice/snow).
8	Barren	Land comprised of natural occurrences of soils, sand, or rocks where less than 10% of the area is vegetated.



Table 2 NLCD land cover cross-walked to LCMAP land cover

NLCD Value	LCMAP Value
Water	Water
Ice/Snow	Ice and Snow
Developed, open space; Developed, low intensity; Developed medium intensity; Developed, high intensity	Developed
Barren	Barren
Deciduous forest, Evergreen forest, Mixed forest	Tree Cover
Shrub/Scrub, Grassland/Herbaceous	Grass/Shrub
Hay/Pasture, Cultivated crops	Cropland
Woody wetland, Emergent herbaceous wetland	Wetland



Table 3. Confusion matrix for CONUS (all years combined) where cell entries represent percent of CONUS area. Overall accuracy is 82.5% ($\pm 0.22\%$). Standard errors for user's and producer's accuracies are shown in parentheses and n is the number of sample pixels for each row and column.

Map	Devel	Crop.	Grass /Shrub	Tree	Water	Wetland	Ice/Snow	Barren	Total	User (SE)	n
Devel.	3.000	0.139	0.321	0.377	0.024	0.035		0.001	3.896	77 (1.2)	32102
Crop.	0.918	16.527	5.061	0.799	0.027	0.368		0.003	23.702	70 (0.6)	195283
Grass /Shrub	0.368	0.757	30.649	2.599	0.045	0.229		0.332	34.980	88 (0.3)	288197
Tree	0.340	0.143	1.414	23.387	0.049	0.579		0.006	25.917	90 (0.3)	213531
Water	0.013	0.008	0.048	0.024	4.788	0.067		0.020	4.968	96 (0.5)	40932
Wetland	0.062	0.129	0.361	0.944	0.172	3.688		0.001	5.357	69 (1.3)	44136
Ice/Snow			0.004	0.004		0.004	0.012	0.004	0.028	43 (18.7)	231
Barren	0.072	0.005	0.501	0.013	0.056	0.012		0.492	1.151	43 (2.8)	9485
Total	4.772	17.707	38.358	28.149	5.162	4.981	0.012	0.859	100.00		
Prod (SE)	63 (1.3)	93 (0.3)	80 (0.4)	83 (0.4)	93 (0.7)	74 (1.2)	100 (0)	57 (3.2)			
n	39319	145886	316027	231916	42530	41042	99	7078			



Table 4 Overall per class agreement in percentage between 1985 and 2017

Overall Per Class Agreement	Developed	Cropland	Grass/Shrub	Tree	Water	Wetland	Snow/Ice	Barren
1985	66	80	83	87	95	72	60	49
1986	67	80	83	87	95	72	60	49
1987	68	80	83	86	95	72	60	49
1988	68	80	83	87	95	72	60	49
1989	68	80	84	87	95	72	60	48
1990	68	80	84	87	95	72	60	48
1991	68	80	84	87	95	72	60	49
1992	69	80	84	87	95	71	60	50
1993	69	80	84	87	95	71	60	49
1994	69	80	84	87	95	71	60	49
1995	70	80	84	87	95	72	60	49
1996	69	80	84	87	95	72	60	48
1997	70	80	84	87	95	72	60	49
1998	70	80	84	87	94	72	60	48
1999	70	80	84	87	95	72	60	48
2000	70	80	84	87	95	72	60	48
2001	70	80	84	87	95	72	60	49
2002	70	80	84	86	95	72	60	49
2003	70	80	84	87	94	71	60	48
2004	69	80	84	86	94	71	60	48
2005	70	80	84	86	94	71	60	49
2006	70	79	84	86	94	71	60	49
2007	70	79	84	86	94	71	60	50
2008	70	79	84	86	94	71	60	49
2009	70	79	84	86	94	71	60	49
2010	70	79	84	86	94	71	60	50
2011	70	79	84	86	94	71	60	51
2012	70	79	83	86	94	71	60	50
2013	69	79	83	86	94	71	60	50
2014	69	79	83	86	94	71	60	50
2015	69	79	83	86	94	71	60	50
2016	69	79	83	86	94	71	60	50
2017	69	78	83	85	94	70	60	49

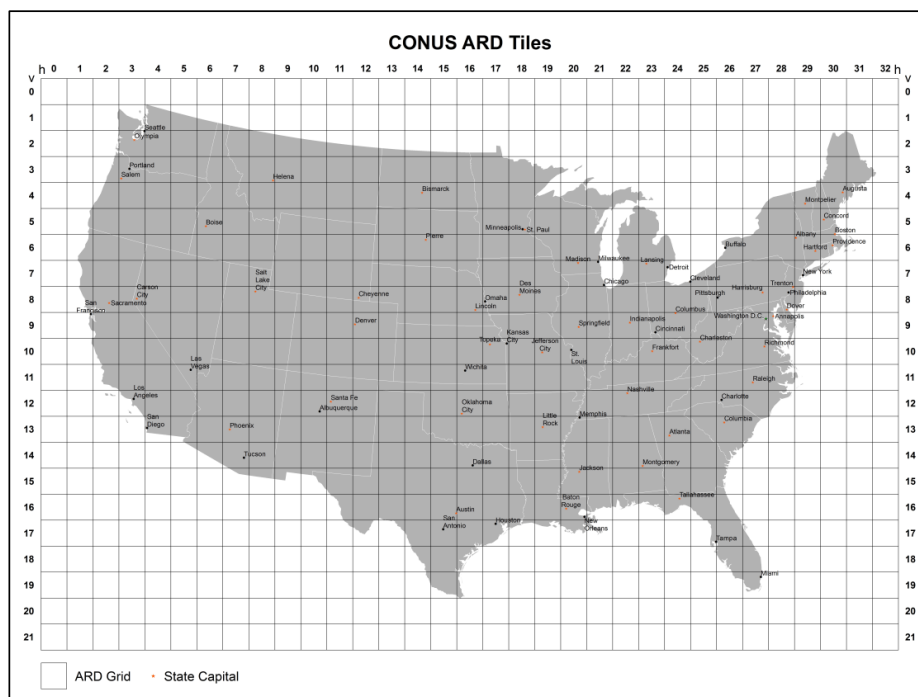


Figure 1 Landsat ARD tile grids for the conterminous U.S.

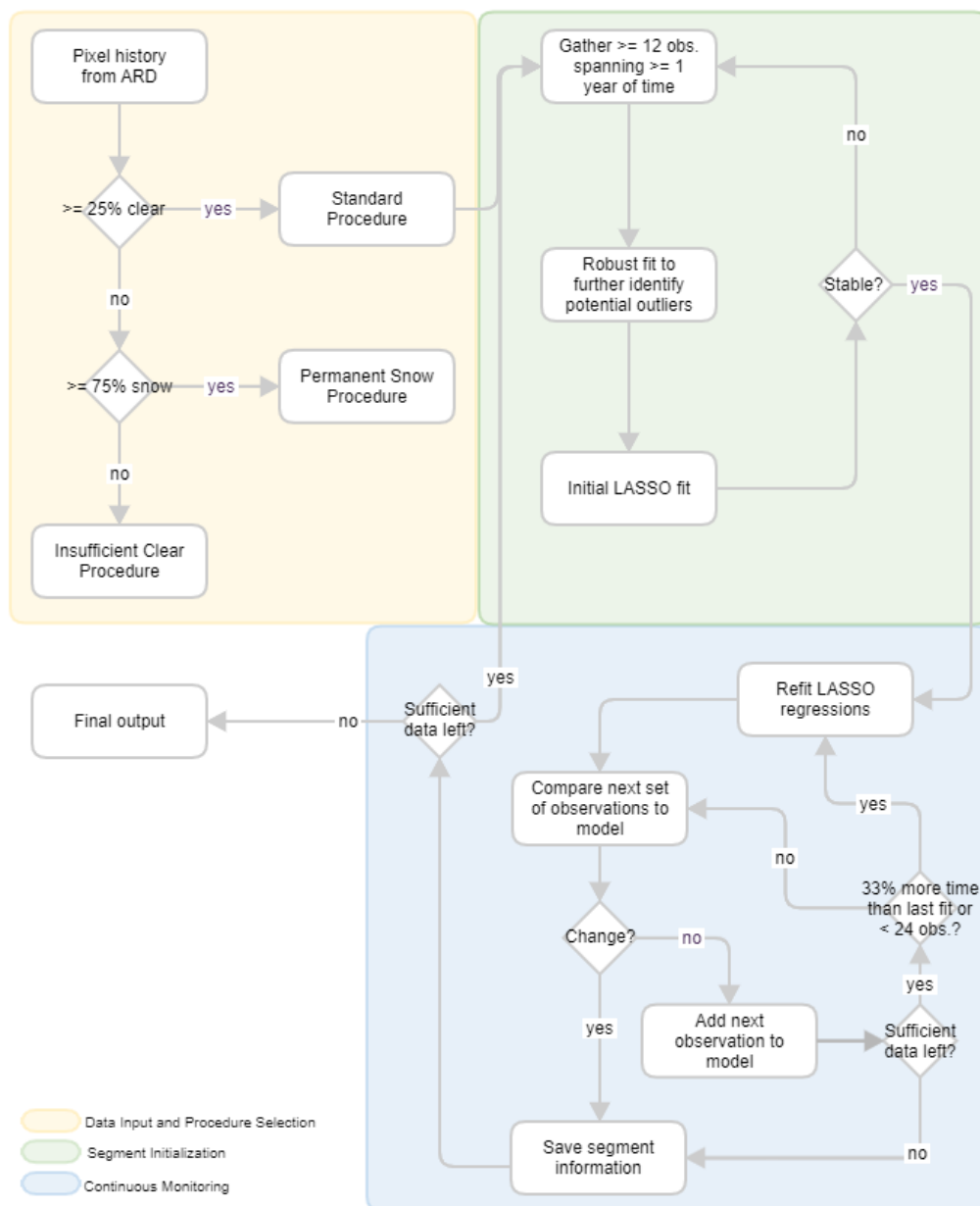


Figure 2 Overall procedures of the CCD algorithm.

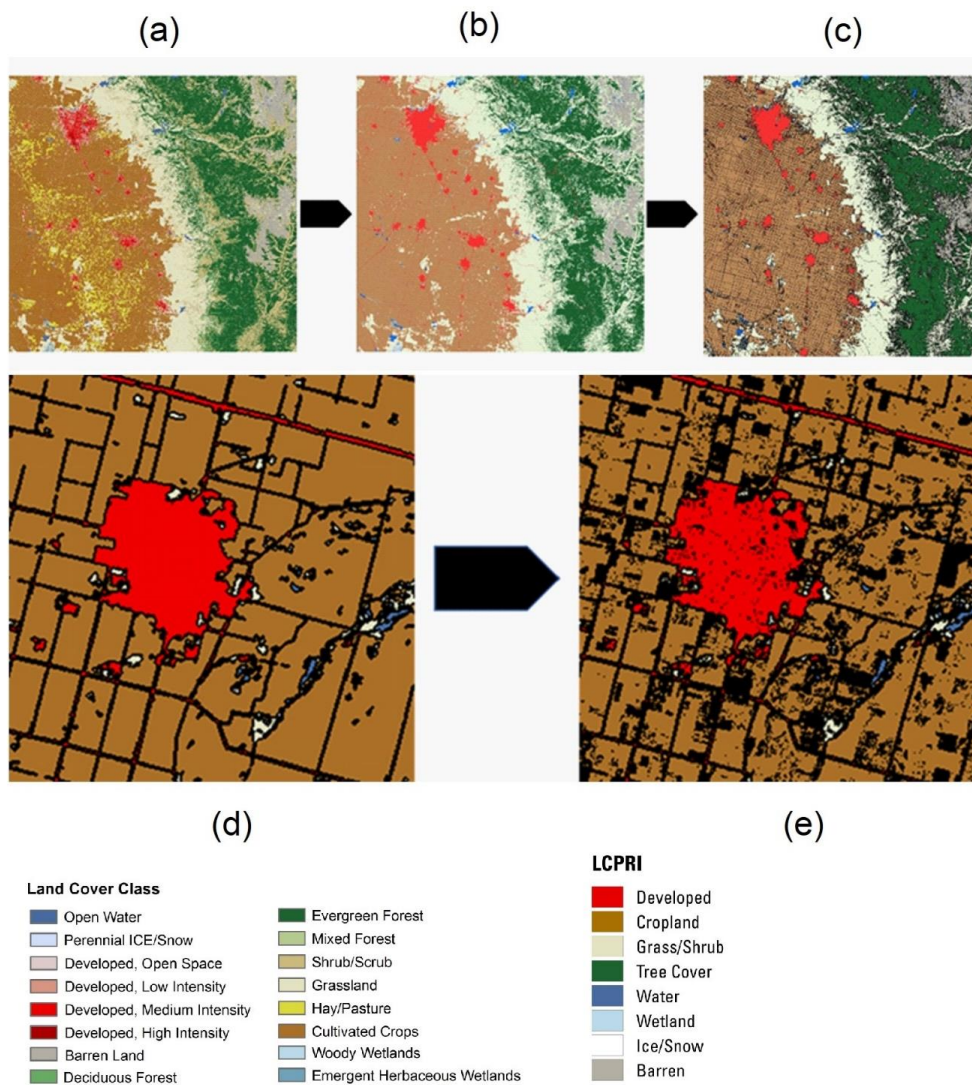


Figure 3. NLCD 2001 land cover (a), cross-walked LCMAP land cover classes (b), LCMAP land cover eroded by one pixel (c), zoomed in cross-walked land cover from NLCD 2001 (d), and zoomed in LCMAP land cover classes eroded by one pixel (e). The color legends represent NLCD land cover class and LCMAP primary land cover (LCPRI).

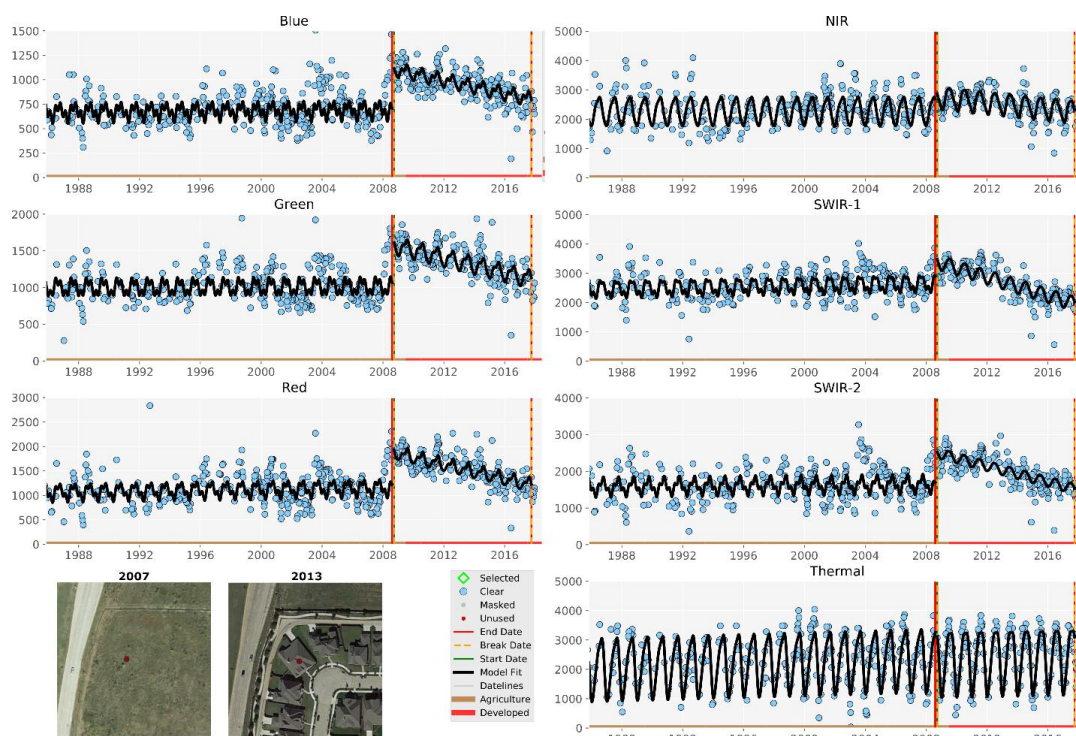


Figure 4 CCD change detection and segmentation using Landsat blue, green, red, near-infrared, short-wave infrared (SWIR) 1, short-wave infrared (SWIR) 2, and thermal bands. Blue dots are all available clear Landsat records in each year. The horizontal lines in different colors represent land cover classes labeled by the algorithm. The vertical lines show model break dates. The back line is the model fits. The high-resolution images show landscape conditions in 2007 and 2013.

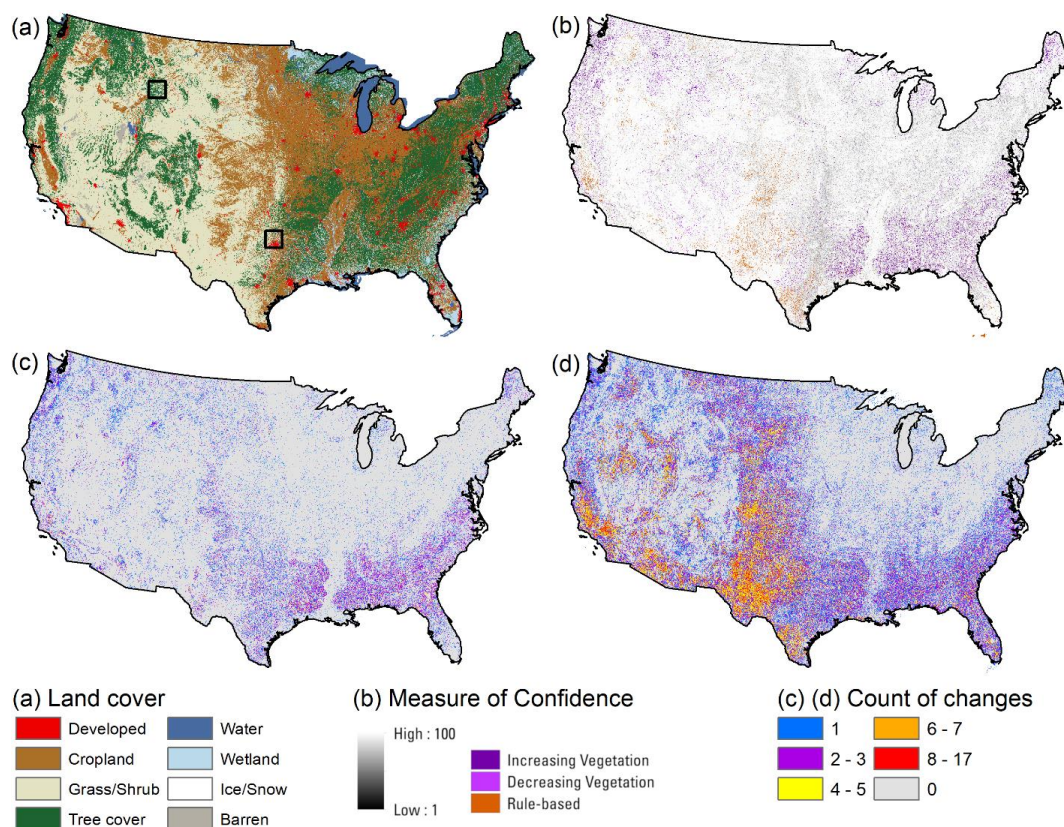


Figure 5 Illustration of the LCMAP product: (a) Primary land cover in 2010, (b) Primary land cover confidence in 2010, (c) total number of land cover changes from 1985 to 2017, and (d) total number of changes detected from 1985 to 2017.

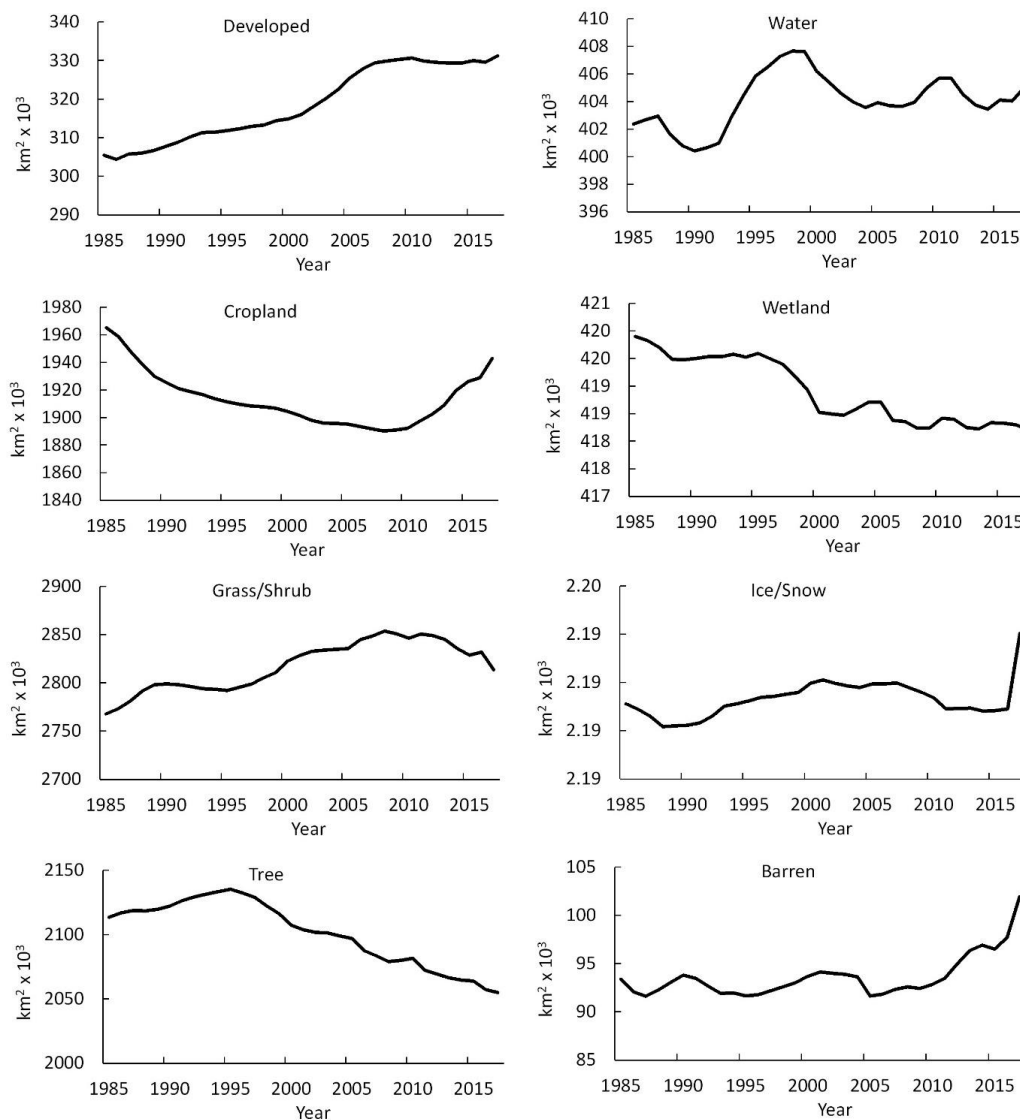


Figure 6 Areal variations of eight primary land cover types from 1985 to 2017 in CONUS.

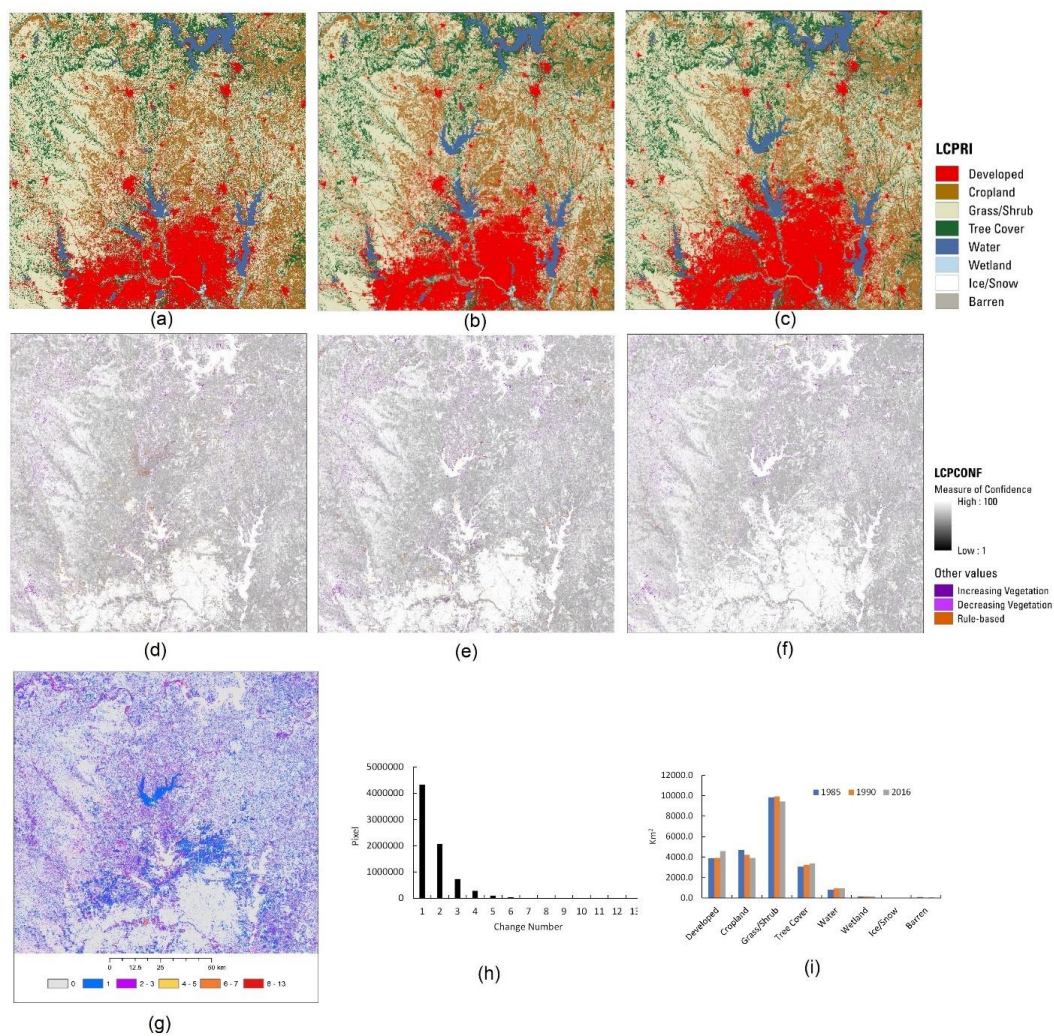


Figure 7 Primary land cover and confidences in 1985 (a) and (d), 1990 (b) and (e), 2016(c) and (f), change in 1985-2017 (g), total pixels of different change (h), and areas of different land cover in the three times for the ARD tile 16_14 (i).

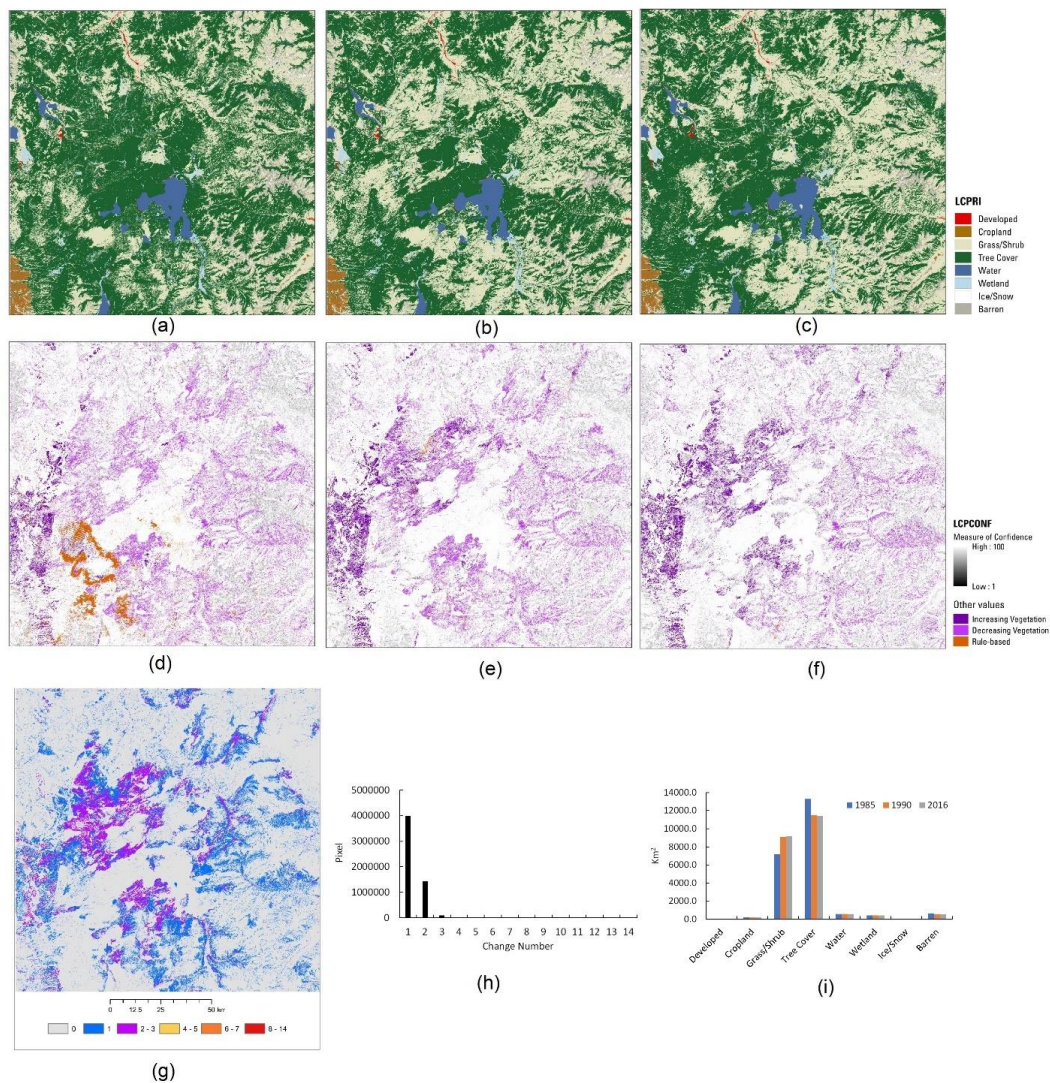


Figure 8 Primary land cover and confidences in 1985 (a) and (d), 1990 (b) and (e), 2016 (c) and (f), and change in 1985-2017 (g), total pixels of different change (h), and areas of different land cover in the three times for the ARD tile9_6 (i).

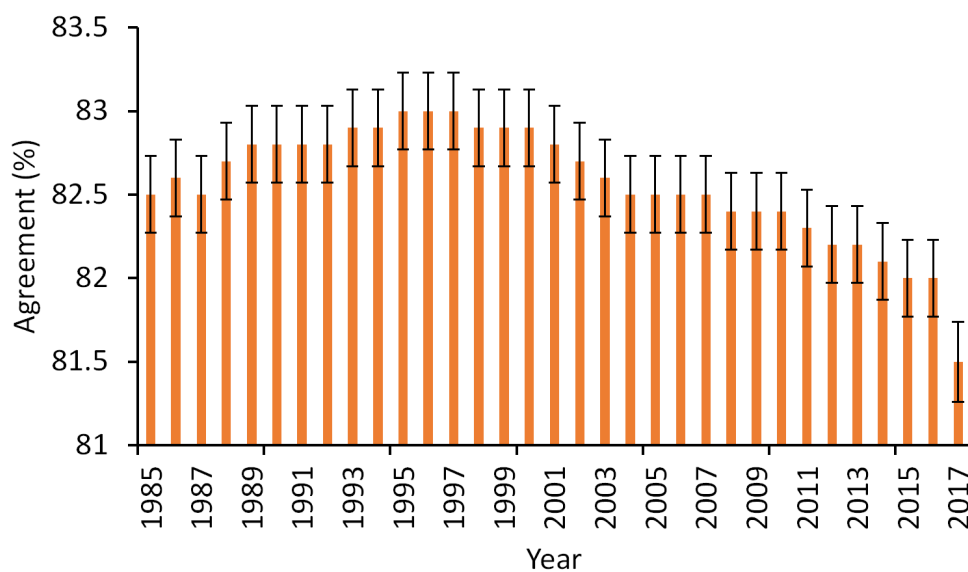


Figure 9 Overall agreement between LCMAP primary land cover and reference data across CONUS. The cross lines represent +/- one standard errors.